Hybrid Grid-Following Control Strategy With DC Inertia Synchronization

Ruixun Ma, Xueguang Zhang, *Member, IEEE*, and Dianguo Xu, *Fellow, IEEE*

***Abstract*—Regarding the subsynchronous oscillation issues of grid-following (GFL) converters in weak grids, existing improved control and parameter optimization strategies are already well-developed. Recent references have proposed hybrid control methods that combine features of GFL and grid-forming (GFM) controls. GFL converters applying a phase-locked loop (PLL) are liable to instability in weak grids, whereas GFM converters exhibit good stability. These hybrid structures focus on the integration of a virtual synchronous generator (VSG) or droop control with GFL control. Apart from VSG and droop control, dc inertia synchronization (IsynC) control is another common GFM strategy. However, there are currently no published references on hybrid control strategies combining GFL control with dc IsynC. Therefore, this article proposes an equivalent hybrid strategy for GFL converters by incorporating dc IsynC. The equivalent hybrid method introduces the dc power deviation to the dc voltage loop output, which will influence the d-axis current directly and q-axis voltage indirectly. Then, the PLL output θ will be consequently affected, and finally, θ will include the same component with IsynC, thereby incorporating the concept of equivalent hybrid dc IsynC. Finally, theoretical analysis and experimental results validate the effectiveness of the proposed equivalent hybrid control strategy.**

***Index Terms*—DC inertia synchronization (IsynC), grid-following (GFL) converter, stability analysis, weak grid.**

I. Introduction

CURRENTLY, the control methods for grid-connected converters mainly consist of two types: grid-following (GFL) control and grid-forming (GFM) control [1], [2], [3]. Typically, GFM relies on a power control as the synchronization unit, whereas GFL uses a phase-locked loop (PLL) to ensure the phase synchronization between the voltage of the point of common coupling (PCC) and the grid voltage. However, GFL control has poor adaptability to the weak grid, in which it is prone to the subsynchronous oscillation (SSO), leading to instability in the grid-connected system [4], [5].

In the weak grid condition, the SSO problem is mainly related to controller bandwidth [6]. As the control bandwidth of the PLL increases, the frequency range of the converter output impedance with negative damping characteristics will also increase. When the magnitude/phase margin of the grid impedance is insufficient, oscillations may occur. Reducing the bandwidth of the PLL within a certain range and increasing the damping ratio of the PLL can improve the stability of the grid-connected system in weak grid conditions [8], however, its effectiveness is usually constrained by the balance between stability margin and dynamic performance [9], [10].

To further enhance the stability of the grid-connected system, various advanced strategies have been proposed. The authors in [12], [13], and [14] proposed the symmetric virtual impedance control aiming at the current loop. Applying supplementary feedforward terms of PCC voltage that result from virtual impedance to the input port of the current loop increases the system damping. The authors in [15], [16], and [17] put feedforward terms arising from PLL into the current loop so that the negative effects of PLL can be eliminated. In [18], forsaking the PI-controlled current loop, an IP controller is used instead, which eliminates the influence of PCC voltage fluctuations on current control in weak grid conditions. In [19], a q-axis voltage-integral damping control independent of PLL parameters and operation points is proposed. As a result, the q-axis voltage is equivalently stiffened, letting the PLL be operated as if the grid were strong.

Apart from the aforementioned modifications to the dual-loop structure, it is also a common way to enhance the stability from the perspective of synchronization unit structures. Lin et al. [20] proposed a new PLL structure, which is achieved by multiplying the PCC voltage by the line impedance and passing it through a band-pass filter. This approach removes the coupling between line impedance and PLL bandwidth and achieves the converter output passive damping, allowing the system to remain stable even with a large PLL bandwidth. Lin et al. [21] proposed a constant-coupling-effect-based PLL to enhance the system synchronization stability, resulting in a low coupling effect between line impedance and PLL bandwidth so that the PLL bandwidth can be designed separately and the system stability is ensured. Mansour et al. [22] proposed a novel PLL structure to eliminate the nonlinear dynamic characteristics of the PLL, utilizing dq-axis voltage and current to construct PLL feedback terms and then expanding the domain of attraction to the whole plane when small disturbances like operating point variations appear.

Different from GFL control, applying PLL, which belongs to the voltage-based synchronization, GFM relying on power-based synchronization will exhibit stronger adaptability to a weak grid. The implementation of GFM control can generally be

Received 9 May 2025; revised 1 August 2025 and 11 October 2025; accepted 25 November 2025. Date of publication 9 December 2025; date of current version 25 February 2026. This work was supported by the National Natural Science Foundation of China under Grant 51977046. Recommended for publication by Associate Editor P. Davari. *(Corresponding author: Xueguang Zhang.)*

The authors are with the Department of Electrical Engineering, Harbin Institute of Technology, Harbin 150000, China (e-mail: 22s006024@stu.hit.edu.cn; zxghit@hit.edu.cn; xudiang@hit.edu.cn).

Color versions of one or more figures in this article are available at https://doi.org/10.1109/TPEL.2025.3641969.

Digital Object Identifier 10.1109/TPEL.2025.3641969

divided into two approaches. The first category is to simulate the rotor equations of synchronous generators (SG) with methods like virtual synchronous generator (VSG). Generating voltage phase and magnitude references by controlling the active and reactive power outer loops, VSG can ensure the stability of converters with a vulnerable grid strength. Another strategy is to establish the inertia relationship between the dc voltage and the grid frequency on the basis of the dc capacitance dynamics. This method imitates the SG via virtual inertia provided by dc capacitance, thereby achieving autonomous synchronization.

Huang et al. [23] adopted a virtual synchronous control method based on dc voltage, in which the deviation of the square of the dc voltage is processed through a first-order transfer function and a first-order integral term to obtain the synchronization angle. Sang et al. [24] first applied inertial synchronization (ISynC) to a grid-connected system with PMSG, letting the dc voltage through a first-order integral term to obtain the synchronization angle. Qin et al. [25] presented another ISynC method using dc voltage deviation through a PI controller to obtain the grid synchronization phase. These dc inertial synchronization strategies exhibit good adaptability to the weak grid.

Based on the different control characteristics of GFL and GFM structures, the idea of hybrid control has been proposed. In terms of hybrid synchronization units, Harnefors et al. [26] integrated GFL control with VSG control, a typical kind of GFM structures, proposing a universal controller structure that combines PLL and active power loop. Based on the research work in [26], Liu et al. [27] introduced an adaptive hybrid control strategy that can adjust the proportion of GFL and GFM according to grid strength, thereby enhancing the stability of the grid-connected converter within a wide range of short-circuit ratios (SCR). Liu and Wang [28] integrated the synchronization structures of VSG and GFL control to propose a composite synchronization control method. By modifying only the synchronization unit, it enhances the stability of the grid-connected systems.

Furthermore, from the perspective of hybrid output variables, Lima et al. [29] combined the output voltage and grid-connected current of VSG and GFL control, scaled by virtual impedance proportions, to generate the modulation voltage, transforming the traditional GFL into hybrid control converters. Han et al. [30] proposed a hybrid strategy combining GFL and GFM with weighted modulation. This control structure replaces the PLL in GFL mode with an active power droop control loop. The outputs of the GFL and GFM current loops are then added after proportional distribution, significantly reducing the negative damping zone of the positive-sequence output impedance, effectively enhancing the stability of the grid-connected converter.

From the aforementioned references, it can be seen that these hybrid control structures focus on combining PLL with the active power synchronization unit of GFM control, including VSG and droop control.

In summary, there exist hybrid control strategies based on GFL control and VSG, but the research on hybrid control combining GFL control and dc inertia synchronization (IsynC) are relatively limited. Therefore, this article invents an equivalent hybrid GFL control strategy with dc power synchronization by introducing dc power disturbance to the voltage loop. With the proposed strategy, the synchronization unit can be equivalent to the result of combining IsynC with PLL, which finally realizes the effect of compound GFM control in the GFL control, so as to strengthen the stability of the GFL converter. Compared to traditional GFL stability optimization strategies [12], [13], [14], [15], [16], [17], [18], [19], [20], [21], the hybrid dc IsynC control strategy proposed in this article adopts a hybrid concept. Compared to existing hybrid control strategies [25], [26], [27], [28], the proposed hybrid dc IsynC control strategy combines GFL with dc IsynC control, presenting a novel GFL/GFM hybrid strategy.

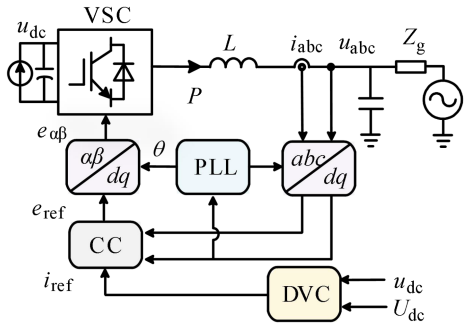

Fig. 1. Topology and control structure of the GFL system.

Combining with the previous work on the dc IsynC control method, this work emphasizes the following:

1) Equivalently, merge GFL control with GFM (dc IsynC) to improve weak-grid stability.
2) Achieve the equivalent hybrid control without modifying the PLL, instead refining the voltage-current loops. The compensation term indirectly embeds dc IsynC into the PLL, enhancing stability while preserving GFL operation.

The rest of this article is organized as follows. The analysis of the synchronization unit structure in traditional GFL control and dc IsynC control is given in Section II. Section III shows the equivalent hybrid GFL control strategy with dc power synchronization and explains the reason for stability improvement. The selection method for control parameters and simulation results is given in Section IV. Experimental results are given in Section V. Finally, Section VI concludes this article.

II. Synchronization Unit Structure of the Grid-Connected Converter System

A. Topology of Traditional GFL Control

The topology of the converter is shown in Fig. 1, in which the machine-side converter is regarded as a current source for convenience. DVC is the dc voltage controller, and C is the current controller. u_{abc} is the PCC voltage, i_{abc} is the grid-connected current, P is the output active power of the converter, and the arrow indicates the direction of power flow. L is the filtering inductance, Z_{g} is the line impedance, and θ is the output angle of the PLL. U_{dc}, i_{ref}, and e_{ref} stand for the reference value for the dc voltage, grid-side current, and the output voltage of the grid-side converter (GSC), respectively. $e_{\alpha\beta}$ is the coordinate

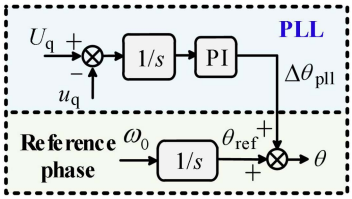

Fig. 2. Control block of synchronization unit in GFL system.

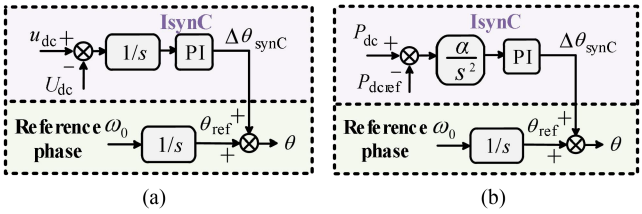

Fig. 3. Synchronization unit structure of IsynC. (a) Fundamental synchronization unit. (b) Equivalent synchronization unit.

transformation result of e_{ref}. u_{dc} and C_{dc} represent the dc bus voltage and dc capacitance.

Traditional GFL control applies the voltage-based PLL as the synchronization unit, as shown in Fig. 2. U_q and u_q stand for the reference value and actual value of the q-axis voltage. ω_0 and θ_{ref} represent the reference value of angular frequency and phase, and $\Delta\theta_{pll}$ is the small-signal form of PLL output angle. However, in the weak grid condition, the PCC voltage is prone to be disturbed, leading to poor adaptability of the grid-connected system with GFL control.

B. DC Inertial Synchronization of GFM Control

Compared to GFL control, GFM control systems exhibit stronger robustness in the low SCR condition. In addition to VSG control, there also exist references studying GFM control methods utilizing the dynamic property of dc capacitance for synchronization. This article selects an IsynC method, which belongs to dc inertial synchronization control for analysis [25]. The diagram of the synchronization unit is shown in Fig. 3(a).

U_{dc} and u_{dc} stand for the steady-state value and actual value of the dc voltage, respectively. $\Delta\theta_{synC}$ is the small-signal form of IsynC output angle.

The expression for deriving the implementation structure of the synchronization unit is shown as follows:

$$\begin{cases}\theta_{synC}=\frac{1}{s}\omega_{synC}\\ \omega_{synC}=(u_{dc}-U_{dc})\cdot(k_{pv}+\frac{k_{iv}}{s})+\omega_0\end{cases}. \tag{1}$$

In the equation, s represents the differential operator, k_{pv} and k_{iv} are parameters of the dc voltage controller. ω_{synC} and θ_{synC} represent the angular frequency and phase of IsynC, respectively.

To establish the relationship between dc voltage and the output phase, we multiply both sides of (1) by the differential operator s, yielding the following equation:

$$s\omega_{synC}=k_{pv}s\left(u_{dc}-U_{dc}\right)+k_{iv}\left(u_{dc}-U_{dc}\right)+s\omega_0. \tag{2}$$

Based on the dynamics of the dc bus capacitor, the relationship between the dc voltage and dc power can be established as

$$P_{dc}=P_s-P_g=U_{dc}C_{dc}s\cdot u_{dc}. \tag{3}$$

Since ω_0 and U_{dc} are constants, their products with the differential operator s become zero. Based on this, combining (2) and (3), we obtained

$$s\omega_{synC}=k_{pv}\frac{P_s-P_g}{U_{dc}C_{dc}}+k_{iv}\left(u_{dc}-U_{dc}\right). \tag{4}$$

Consequently, we obtain the following equation:

$$\frac{U_{dc}C_{dc}}{k_{pv}}s\omega_{synC}=P_s-P_g+\frac{k_{iv}U_{dc}C_{dc}}{k_{pv}}\left(u_{dc}-U_{dc}\right). \tag{5}$$

In (5), P_s and P_g represent the output power of the dc side and GSC, respectively. P_g can also be expressed as

$$P_g=\frac{U_fU_g}{X}\sin\delta. \tag{6}$$

In (6), U_f is the output voltage of GSC. U_g is the grid voltage. X represents the sum of the filtering inductance and the line inductance. δ is the phase deviation between U_f and U_g.

Combining with (5) yields the final form of the IsynC synchronization equation

$$\begin{cases}\theta_{synC}=\frac{1}{s}\omega_{synC}\\ \frac{C_{dc}U_{dc}}{k_p}s\omega_{synC}=P_s-\frac{U_fU_g}{X}\sin\delta+\frac{k_{iv}U_{dc}C_{dc}}{k_{pv}}\left(u_{dc}-U_{dc}\right)\end{cases}. \tag{7}$$

Sang et al. [24] suggested that the dynamic variation of dc voltage can be neglected in steady-state conditions, ultimately yielding the following equation:

$$\begin{cases}\theta_{synC}=\frac{1}{s}\omega_{synC}\\ \frac{C_{dc}U_{dc}}{k_p}s\omega_{synC}=P_s-\frac{U_fU_g}{X}\sin\delta\end{cases}. \tag{8}$$

The expression for the rotor motion equation of a synchronous generator can be described as

$$\begin{cases}\theta_s=\frac{1}{s}\omega_s\\ J_ss\omega_s=P_m-P_e-D_s\left(\omega-\omega_0\right)\end{cases} \tag{9}$$

where J_s and D_s represent the inertia and damping coefficient of the synchronous generator, respectively. ω_s and θ_s are the angular frequency and phase of the synchronous machine, respectively. P_m and P_e represent the input and output power of the synchronous machine, respectively.

Comparing (8) with (9), it is apparent that they have nearly identical forms. Therefore, the IsynC strategy can apply the dynamic of the dc capacitance to active power control, thereby generating the frequency and phase.

Express the IsynC phase equation and the dc power equation in the small-signal form

$$\begin{cases}\Delta\theta_{synC}=\Delta u_{dc}\cdot\left(k_{pv}+\frac{k_{iv}}{s}\right)\frac{1}{s}\\ \Delta P_{dc}=U_{dc}C_{dc}s\cdot\Delta u_{dc}\end{cases}. \tag{10}$$

Then the relationship between the output angle and the dc power can be obtained. The equivalent control diagram of the synchronization unit is shown in Fig. 3(b), in which P_{dc} and

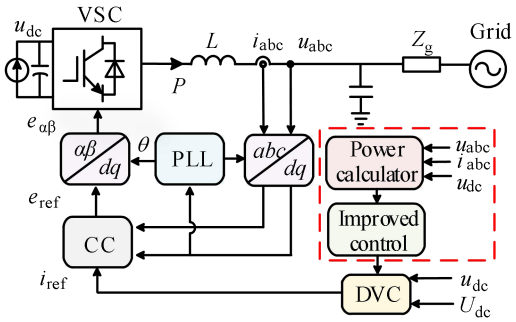

Fig. 4. Overall block diagram of hybrid synchronization control.

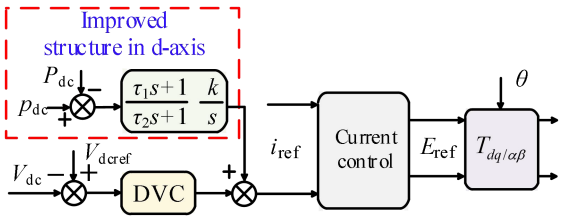

Fig. 5. Detailed structure of equivalent hybrid synchronization control.

P_{dcref} stand for the steady-state value and actual value of the dc voltage and $\alpha = 1/U_{\mathrm{dc}}C_{\mathrm{dc}}$.

$$\Delta\theta_{\mathrm{synC}} = \Delta P_{\mathrm{dc}} \cdot \left(k_{\mathrm{pv}} + \frac{k_{\mathrm{iv}}}{s}\right) \cdot \frac{1}{U_{\mathrm{dc}}C_{\mathrm{dc}}s^2}. \tag{11}$$

III. Equivalent Hybrid Grid-Following Converter Strategy With DC Inertia Synchronization

In weak grids, GFL control is prone to SSO risks. Existing references indicate that the stability of GFL inverters in weak grids is primarily influenced by the PLL bandwidth and line impedance. To address this problem, this article proposes an equivalent hybrid dc power synchronization control, which effectively combines GFL and GFM control strategies, thereby resolving SSO issues in GFL inverters under conditions of low SCR and high PLL bandwidth.

Based on the analysis of the IsynC strategy in Section II, this article proposes a novel hybrid dc power synchronization strategy for the GFL converter to enhance the stability of the grid-connected system in weak grid conditions. The overall diagram of the equivalent hybrid synchronization control is shown in Fig. 4, and the detailed diagram is shown in Fig. 5.

Since the GFL control structure relies on the dc voltage outer loop to generate current references, directly injecting an additional term derived from the dc voltage might cause control conflicts and potential system instability. To mitigate this issue, this article first converts dc voltage synchronization into dc power synchronization and then uses the resulting dc power, rather than the dc voltage directly, to generate the compensation term.

The deviation of dc power is introduced into the dc voltage loop output through a lead/lag transfer function and an integrator. τ_1 and τ_2 are time constants of the lead/lag transfer function, and k is the proportional coefficient of the equivalent hybrid synchronization control. $T_{\mathrm{dq}/\alpha\beta}$ is the coordinate transformation module.

According to the structure shown in Fig. 5, the improved control equation for the d-axis of the GSC can be derived as

$$\begin{cases} x = (P_{\mathrm{dc}} - P_{\mathrm{dcref}}) \cdot \frac{\tau_1 s+1}{\tau_2 s+1} \cdot \frac{k}{s} \\ i_{\mathrm{dref}}{}' = i_{\mathrm{dref}} + x \end{cases} \tag{12}$$

where x represents the output obtained by the dc power deviation through the improved function. i_{dref} is the original d-axis current reference value. i_{dref}' is the updated d-axis current reference value after introducing x.

Due to the existence of the current loop PI section, the d-axis current will also change with the reference value.

$$\begin{cases} i_{\mathrm{d}}{}' = i_{\mathrm{dref}}{}' \\ \Delta x = \Delta P_{\mathrm{dc}} \cdot \frac{\tau_1 s+1}{\tau_2 s+1} \cdot \frac{k}{s} \\ \Delta i_{\mathrm{d}}{}' = \Delta i_{\mathrm{d}} + \Delta x \end{cases} \tag{13}$$

where i'_d is the new d-axis current after introducing x. The symbol Δ denotes the small-signal form of variables.

The relationship between grid voltage, grid impedance, and PCC voltage can be expressed as

$$\begin{cases} u_{\mathrm{d}} = u_{\mathrm{gd}} - R_{\mathbf{g}} i_{\mathrm{d}} + \omega_{\mathbf{g}} L_{\mathbf{g}} i_{\mathrm{q}} \\ u_{\mathrm{q}} = u_{\mathrm{gq}} - R_{\mathbf{g}} i_{\mathrm{q}} - \omega_{\mathbf{g}} L_{\mathbf{g}} i_{\mathrm{d}} \end{cases} \tag{14}$$

where u_{dq} and i_{dq} represent the dq-axis component of the three-phase PCC voltage and current. u_{gdq} represents the dq-axis component of the grid voltage. ω_{g} is the grid frequency. R_{g} and L_{g} represent the line impedance.

Typically, the reactance of the line is much larger than the resistance. Neglecting the line resistance, the small-signal expression for the q-axis voltage can be obtained as

$$\Delta u_{\mathrm{q}} = \Delta u_{\mathrm{gq}} - \omega_{\mathbf{g}} L_{\mathbf{g}} \Delta i_{\mathrm{d}}. \tag{15}$$

The small-signal component of constant grid voltage can also be ignored. Combining (14) and (15), it can be observed that the introduction of equivalent hybrid synchronization control will affect the active current, thereby influencing the small-signal form of the q-axis voltage as follows:

$$\Delta u_{\mathrm{q}}{}' = -\omega_{\mathbf{g}} L_{\mathbf{g}} (\Delta i_{\mathrm{d}} + \Delta x) \tag{16}$$

where $\Delta u_{\mathrm{q}}{}'$ represents the small-signal component of the new q-axis voltage after the introduction of improved control.

According to the relationship between Δu_{q} and the phase in GFL control, the small-signal expression of the angle $\Delta\theta'$ can be obtained

$$\begin{aligned} \Delta\theta' &= -\Delta u_{\mathrm{q}}{}' \left(k_{\mathrm{ppll}} + \frac{k_{\mathrm{ipll}}}{s}\right) \frac{1}{s} \\ &= \Delta\theta_{\mathrm{pll}} + \omega_{\mathbf{g}} L_{\mathbf{g}} \Delta x \cdot \left(k_{\mathrm{ppll}} + \frac{k_{\mathrm{ipll}}}{s}\right) \frac{1}{s} = \Delta\theta_{\mathrm{pll}} + \Delta\theta_{\mathrm{x}} \end{aligned} \tag{17}$$

where $\Delta\theta_{\mathrm{pll}}$ is the small-signal value of the PLL output angle. $\Delta\theta_{\mathrm{x}}$ is the small-signal value of the improved control output angle, and k_{ppll} and k_{ipll} are the control parameters of the PLL.

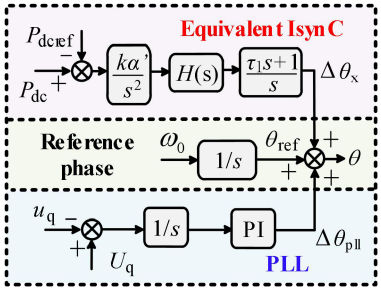

Fig. 6. Equivalent block diagram of equivalent hybrid synchronization control.

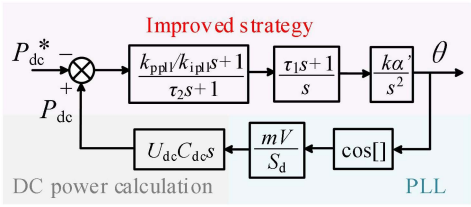

Fig. 7. Closed control loop of equivalent hybrid synchronization control.

Finally, the expression for $\Delta\theta_x$ can be deduced as

$$\begin{aligned}\Delta\theta_x &= \omega_g L_g \frac{\tau_1 s+1}{\tau_2 s+1}\cdot\frac{k}{s}\cdot\frac{k_{ppll}s+k_{ipll}}{s}\cdot\frac{1}{s}\cdot\Delta P_{dc}\\ &= \Delta P_{dc}\cdot\frac{\tau_1 s+1}{\tau_2 s+1}\cdot\frac{\omega_g L_g k}{s^2}\left(k_{ppll}+\frac{k_{ipll}}{s}\right)\\ &= \Delta P_{dc}\cdot\left(\tau_1+\frac{1}{s}\right)\cdot\frac{\omega_g L_g k_{ipll} k}{s^2}\cdot H(s)\end{aligned} \tag{18}$$

where $H(s)=\frac{k_{ppll}s/k_{ipll}+1}{\tau_2 s+1}$.

Comparing (11) with (18), the small-signal angle value introduced by the equivalent hybrid synchronization control has a similar form to that of IsynC. If the time constant τ_2 of the lead/lag function is equal to the ratio of the proportional and integral coefficients of the PLL, H(s) can be ignored, and then the expression of $\Delta\theta_x$ is identical to that of $\Delta\theta_{synC}$.

Based on the above analysis, the impact of the improved control on the grid-connected system can be illustrated. The dc power affects the q-axis voltage through the voltage and current loops and then influence the output of the PLL. Finally, θ includes the components of both PLL and IsynC synchronization unit, thereby compounding the GFL control with GFM control.

Therefore, an equivalent block diagram of equivalent hybrid control can be obtained as shown in Fig. 6, in which $\alpha' = k_{ipll}\omega_g L_g$.

The small-signal angle value caused by equivalent hybrid power synchronization control can be equivalent to the result of combining the IsynC of GFM with the PLL of GFL. This ultimately achieves the effect of compound GFM control in the GFL control, thereby enhancing the stability of the grid-connected system in weak grid conditions.

Thus, the proposed equivalent hybrid dc IsynC does not directly modify the fundamental structure of the PLL but can ultimately achieve an effect equivalent to introducing GFM synchronization characteristics into the synchronization unit of GFL converters. This effectively enhances the stability of GFL converters under weak grid conditions.

IV. Parameter Selection Criteria and Stability Analysis

To ensure that the equivalent hybrid synchronization control effectively enhances the stability of the system, it is necessary to determine the parameters of the equivalent hybrid synchronization control reasonably. Thus, in this section, based on the equivalent hybrid synchronization control structure, a parameter tuning scheme is proposed, and the influence of the equivalent hybrid synchronization control on the system stability is analyzed by root locus analysis.

A. Parameter Selection for the Equivalent Hybrid Control

At steady state, the relationship between the d-axis output voltage and dc voltage can be expressed as

$$u_{dc} = \frac{e_d}{s_d} \tag{19}$$

where e_d represents the output voltage of the d-axis, and s_d denotes the duty cycle of the d-axis. Based on the current loop equation, the relationship between e_d and u_d can be obtained

$$e_d = u_d + \omega_g L i_q \tag{20}$$

Based on (2) and (18)–(20), the closed control loop of the improved method is shown in Fig. 7.

V represents the magnitude of the grid voltage, m is the ratio of e_d and u_d in the steady state.

Hence, after the linearization, the open-loop transfer function $W_{oc}(s)$ can be obtained

$$W_{oc}(s) = \frac{k\alpha' mVC_{dc}U_{dc}(\tau_1 s+1)(\tau_\theta s+1)}{S_d s^2(T_s s+1)(\tau_2 s+1)} \tag{21}$$

$\tau_\theta = k_{ppll}/k_{ipll}$, T_s represents the sampling time, and $T_s = 1$ ms is selected.

For the ease of analysis, we can choose the value of τ_2 close to τ_θ, which simplifies the higher-order system.

$$W_{oc}(s) = \frac{k\alpha' VC_{dc}U_{dc}(\tau_1 s+1)}{S_d s^2(T_s s+1)}. \tag{22}$$

The tuning of the parameters for the hybrid synchronization control should focus on antidisturbance performance. Therefore, the parameters can be designed according to the typical type II system. Then yield the midbandwidth h_v as follows:

$$h_v = \frac{\tau_1}{T_s}. \tag{23}$$

Given the typical relationship of type II systems, the relationship among parameters is shown in (20)

$$\frac{k\alpha' VC_{dc}U_{dc}}{S_d} = \frac{h_v+1}{2h_v^2 T_s}. \tag{24}$$

Taking into account both antidisturbance and tracking ability of the control system, typically choose $h_v = 5$.

TABLE I
PARAMETERS AND VALUES

Parameter	Value	Parameter	Value
Grid voltage u_g/V	95	PLL parameter k_{ipll}	4.4
Output voltage E_d/V	78	CC parameter k_{pi}	0.02
Line impedance L_g/mH	16	CC parameter k_{ii}	0.4
Filter impedance L_f/mH	7	DVC parameter k_{pu}	0.1
Filter capacitance C_f/uF	3.3	DVC parameter k_{iu}	0.5
DC capacitance C_{dc}/mF	2.24	time constant τ_1	0.005
DC voltage U_{dc}/V	200	time constant τ_2	0.0625
PLL parameter k_{ppll}	0.28	proportional coefficient k	0.0625

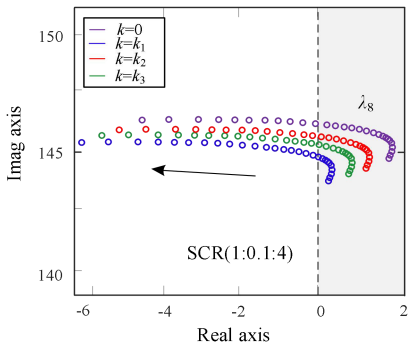

Fig. 8. Root locus of eigenvalue related to SSO mode when increasing SCR with different values of k.

Finally, the theoretical value of parameters can be derived as

$$\begin{cases} \tau_1 = 5T_s \\ k = \frac{3S_d}{25T_s C_{dc} U_{dc} \alpha' V} \\ \tau_2 = \tau_\theta \end{cases}. \tag{25}$$

B. Stability Analysis of Equivalent Hybrid Control With Different Parameters

To demonstrate the effectiveness of equivalent hybrid synchronization control on the stability enhancement of GSC and the rationality of the selection method for parameters, this section conducts stability analysis of the root locus based on the established state space model. According to the distribution of root locus, the eigenvalues corresponding to the SSO mode are $\lambda_{8,9}$. Therefore, this section will focus on the analysis of $\lambda_{8,9}$.

According to the parameters in Table I and (21), the optimal value of k is 0.0625 ($k_{optimal}$). Select $k_0 = 0$, $k_1 = k_{optimal}$, $k_2 = 0.5k_{optimal}$, and $k_3 = 2k_{optimal}$, and then conduct the comparative analysis.

Fig. 8 shows the root locus of λ_8 with different values of the equivalent hybrid control coefficient k as the SCR changes. According to the overall trend of the root locus, it is obvious that increasing the SCR can improve the system stability, as λ_8 gradually moves from the right half-plane to the left half-plane with the increase of SCR.

In the operating condition corresponding to Table I, the addition of equivalent hybrid control with appropriate parameters ($k = k_1$, blue) can broaden the stable operation limitation of SCR, indicating that the inclusion of the proposed control can enhance the stability of the grid-connected system with a lower SCR. However, when the value of k is too small ($k = k_2$, red) or too large ($k = k_3$, green), the effectiveness of equivalent hybrid power synchronization control is reduced.

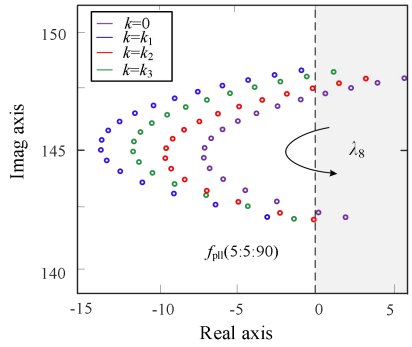

Fig. 9. Root locus of eigenvalue related to SSO mode when increasing f_{pll} with different values of k.

When equivalent hybrid dc IsynC control is not applied, the stability boundary SCR of the GFL converter is 3. With the introduction of dc IsynC control ($k = k_{optimal}$), the stability boundary SCR of the GFL converter is 2.3. With the introduction of dc IsynC control ($k = 0.5k_{optimal}$), the stability boundary SCR of the GFL converter is 2.7. With the introduction of dc IsynC control ($k = 2k_{optimal}$), the stability boundary SCR of the GFL converter is 2.5.

Since the controller parameters in the theoretical analysis are relatively small values, the inherent stability of the GFL system itself is weak. However, the SCR boundary shows significant improvement after introducing the enhanced control. If more optimized controller parameters were selected in the simulation, the stability boundary SCR of the GFL converter with the improved control could have even lower values, thus verifying the effectiveness of the equivalent hybrid dc IsynC strategy.

Fig. 9 shows the root locus of λ_8 with different values of k as f_{pll} changes (SCR = 2). According to the overall moving trend of the eigenvalue, an appropriate increase in f_{pll} can improve system stability. However, if f_{pll} is too large, it can also make the system prone to instability. λ_8 gradually moves from the right half-plane to the left half-plane and then back to the right half-plane with the continuous increase of f_{pll}.

In the operation condition corresponding to Table I, the stable operation range of f_{pll} is widened after the introduction of equivalent hybrid control with proper control parameters ($k = k_1$, blue). Therefore, it indicates that equivalent hybrid power synchronization control can suppress the instability caused by increasing the bandwidth of PLL.

However, when k is too small ($k = k_2$, red) or too large ($k = k_3$, green), the effectiveness of stability enhancement will decrease.

The above root locus analysis demonstrates that equivalent hybrid synchronization control can promote the stability of the grid-connected system. However, when the deviation between the selected parameters of the equivalent hybrid control and the theoretical value $k_{optimal}$ is too large, the effectiveness of stability enhancement will be weakened. The specific values

TABLE II
PARAMETERS OF GRID-CONNECTED SYSTEM

Parameter	Value	Parameter	Value
CC parameter k_{pi}	4	DVC parameter k_{pu}	0.2
CC parameter k_{ii}	32	DVC parameter k_{iu}	3.2

need to be reasonably chosen based on actual application occasions.

The proposed equivalent hybrid dc power synchronization structure differs from existing approaches (such as the strategies in references [9], [12], [17], [26]) in terms of control performance, robustness, and implementation complexity. This method requires fewer injection points for additional terms and a smaller number of designed parameters. Moreover, it preserves the original synchronization unit architecture and achieves equivalent hybrid control by modifying terms within the dc voltage loop, thereby reducing potential instability risks associated with direct PLL alterations under weak grid conditions.

It should be noted that this study focuses on introducing a novel equivalent hybrid control strategy as an advanced alternative, rather than demonstrating substantial performance improvements over existing methods. Both conventional control techniques and the proposed equivalent hybrid dc power synchronization can improve the adaptability of GFL converters in weak grids. The selection of an appropriate control strategy should be application-specific, taking into account operational requirements, grid-connected hardware parameters, and internal control structure and tuning.

C. Simulation Verification

To attest the effectiveness of the stability enhancement of equivalent hybrid power synchronization control, this section conducts the simulations.

To validate the effectiveness of the proposed control strategy, this article conducts theoretical analysis and simulations under various operating conditions. The corresponding control parameters are listed in Table II, whereas all other hardware parameters remain consistent with those in Table I.

In Fig. 10, the purple root locus corresponds to the SSO mode of the GFL converter without the proposed control. The blue root locus represents the GFL converter with the improved control, using parameters selected according to the proposed design.

As shown in Fig. 10 (purple curve), when the PLL bandwidth is 20 Hz, the characteristic roots lie in the left half-plane, indicating system stability. When the PLL bandwidth increases to 85 Hz, the roots shift to the right half-plane, causing instability, with an oscillation frequency of 12.8 Hz (as indicated by the imaginary axis).

As shown in Fig. 10 (blue curve), the GFL converter remains stable at both 20 and 85 Hz PLL bandwidths, with all characteristic roots staying in the LHP, which confirms that the proposed control effectively suppresses SSOs induced by higher PLL bandwidths.

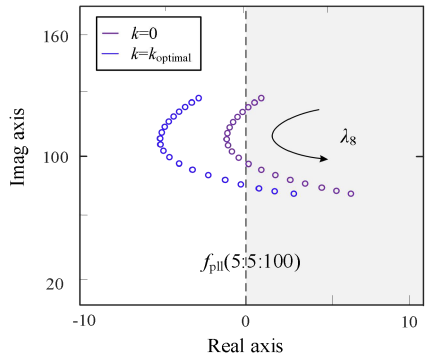

Fig. 10. Root locus of eigenvalue related to SSO mode when increasing f_{pll} with different values of k.

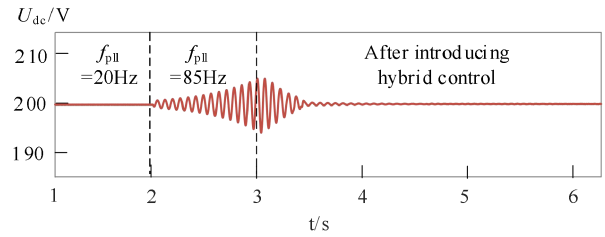

Fig. 11. Simulation result of DC voltage.

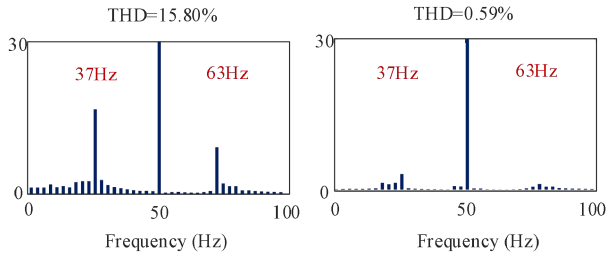

Fig. 12. FFT analysis results of grid-side current.

The simulation scenario of Fig. 11 involves increasing the PLL bandwidth from 20 to 85 Hz, leading to 13 Hz SSOs and system instability, which is consistent with the red root locus. After introducing the equivalent hybrid dc IsynC control with tuned parameters. The oscillations dampen, and the system regains stability within 0.5 s, aligning with the stability enhancement predicted by the blue root locus.

As shown in Fig. 12, the THD of three-phase current has decreased from 15.80% to 0.59%, testifying the obvious effect of the proposed strategy.

Fig. 13 shows the simulated results of the dc voltage u_{dc} with different values of k. Increasing the bandwidth of the PLL, the GFL system appears SSO, and then introduces the equivalent hybrid strategy. When $k = 0.5k_{\mathrm{optimal}}$, the oscillation was suppressed slowly. Then, let $k = k_{\mathrm{optimal}}$, the speed of suppression is fast, and the oscillation has been mitigated. However, when $k = 2k_{\mathrm{optimal}}$, which is too large, the system becomes unsteady again, verifying that the equivalent hybrid control parameter

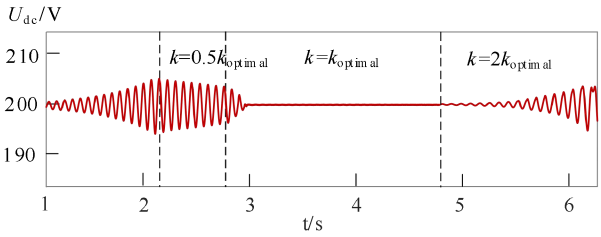

Fig. 13. Simulation result of DC voltage with different k.

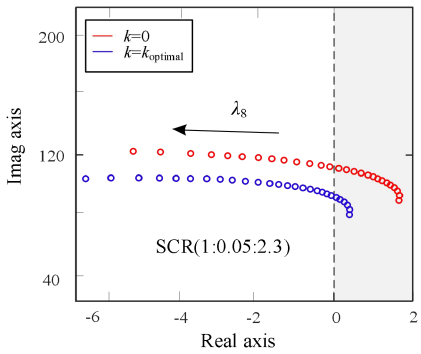

Fig. 14. Root locus of λ_8 before and after adding advanced control when SCR changes.

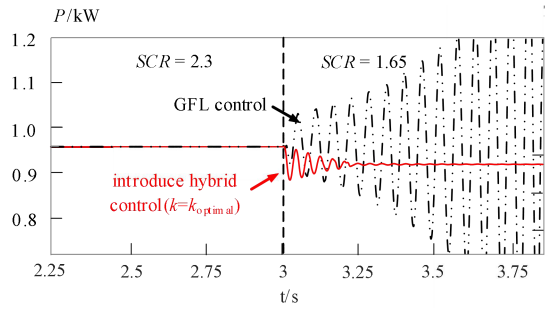

Fig. 15. Simulation result of active power before and after adding advanced control when facing a sudden decrease of SCR.

should be selected within a reasonable range according to the operation condition.

Fig. 14 shows the root locus curves of $\lambda_{8,9}$ when changing the system's SCR. The red curve corresponds to the GFL system without the improved control, while the blue curve represents the GFL system with the equivalent hybrid control using properly selected parameters. From the overall trend of the root locus curves, it can be observed that as the SCR increases, $\lambda_{8,9}$ gradually move from the right half-plane to the left half-plane, indicating improved stability of the GFL converter system. Comparing the red and blue curves reveals that the traditional GFL control has a stable operating SCR boundary of 1.65, whereas the GFL converter with the improved control has a stable SCR boundary of 1.35. This proves that the equivalent hybrid power synchronization control enhances the system stability of GFL converters in weak grid conditions.

Based on the aforementioned theoretical analysis, to validate the effectiveness of equivalent hybrid dc IsynC control in enhancing the stability of GFL converters under weak grid conditions, this study establishes a simulation model.

Fig. 15 shows the active power simulation waveforms when the SCR of the GFL converter abruptly changes from 2.3 to 1.65. The black curve represents traditional GFL control, while the red curve corresponds to the equivalent hybrid dc IsynC control structure. During stable system operation, $L_g = L_{g1}$ (13.5 mH), time constants τ_1 and τ_2, and compensation coefficient $k_{optimal}$ are all zero; the SCR of the system is 2.3. The line inductance switches to $L_g = L_{g2}$ (19 mH) at 4 s of the simulation, changing SCR to 1.65. The results demonstrate that when the SCR suddenly decreases, the grid-connected system with traditional GFL control (black curve) exhibits severe power oscillations leading to instability. In contrast, the system incorporating equivalent hybrid dc IsynC control shows damped oscillations during the transition and quickly regains stability, proving that the equivalent hybrid dc inertia control effectively improves the GFL converter's adaptability to weak grid conditions.

Therefore, the validation of the proposed strategy has been verified by simulation results. For further attestation, the experiments will be conducted in the next section.

D. Differences Among the Proposed Method and Existing Strategies

Unlike existing research that primarily focuses on voltage and current loop compensation terms and the concept of composite ac power synchronization, this study innovatively introduces an equivalent dc power synchronization mechanism indirectly into the synchronization process of GFL converters. This provides a new approach to suppressing SSOs in weak grids and enriches the theoretical framework of hybrid control.

The research works presented in [12], [13], [14], [15], [16], [17], [18], and [19] presented stability improvement methods based on additional voltage and current loop components, whereas the research works presented in [26], [27], and [28] proposed stability enhancement methods combining PLL synchronization with power synchronization techniques. However, the supplementary terms introduced in these methods all use ac-side variables as input quantities, without considering control variables from the dc side. Therefore, compared to existing improved control methods, this strategy utilizes dc power as the input variable, resulting in structural differences from existing methods in terms of implementation, with distinct characteristics in parameter design and performance.

The equivalent dc power composite synchronization strategy structurally employs dc power as the core control variable. This variable can rapidly reflect grid state changes through dc dynamics. Since this method differs in control structure from the methods in references [12], [13], [14], [15], [16], [17], [18], [19], [26], [27], [28], their performance variations depend on parameter designs of system control links and filtering components. For different converter operating conditions, with proper system parameter design, the improved control methods all exhibit good steady-state accuracy and dynamic response characteristics,

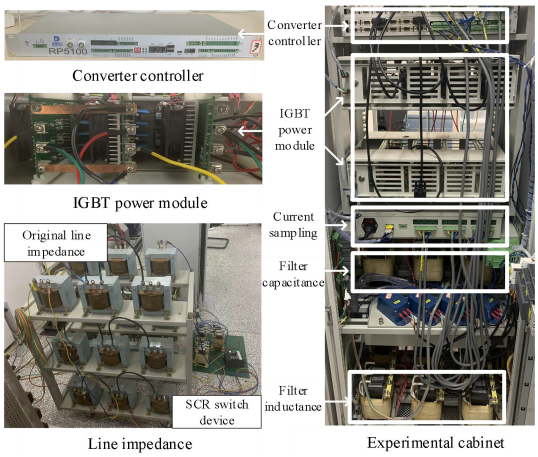

Fig. 16. Grid-connected system experimental platform.

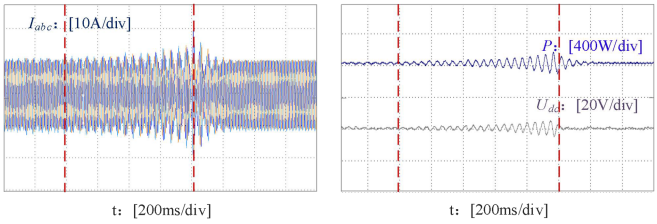

Fig. 17. Experimental results of the weak grid (SCR = 1.8) with a PLL bandwidth step change and then applying the equivalent hybrid control.

effectively enhancing the stability of grid-connected converters in weak grids.

V. Experimental Verification

To validate the effectiveness of the proposed equivalent hybrid dc power synchronization control strategy, the experiments are conducted by the platform shown in Fig. 16. The controller core of the experimental platform is TMS320F28377DZWT, and the hardware part of the experimental platform includes IGBT power modules, filtering inductance, filtering capacitance, line impedance, and isolation transformers, constructing an LCL converter model. To simulate weak grid conditions, the grid impedance of 12 mH is selected. The parameters of the platform are listed in Table I.

The increase of PLL bandwidth is likely to trigger SSO in the weak grid condition. To verify the stability enhancement effect of the equivalent hybrid power synchronization strategy, the experimental results of the i_{abc} and P before and after the implementation of the equivalent hybrid synchronization strategy with the same operating conditions are compared, as shown in Fig. 17.

To facilitate experimental implementation, the small-signal value of dc power can be obtained by subtracting the low-pass-filtered actual dc power from its original value, preserving the dynamic characteristics of dc power while obtaining the small-signal component. This approach only requires designing a sufficiently low cutoff frequency.

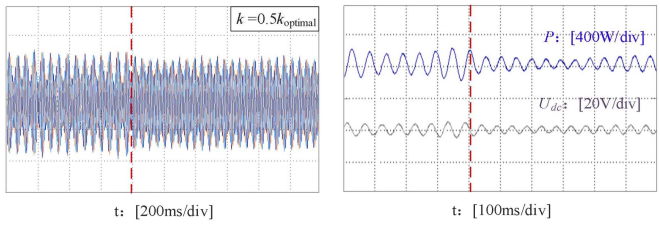

Fig. 18. Effect of equivalent hybrid synchronization control with unreasonable parameter ($k = 0.5k_{\mathrm{optimal}}$).

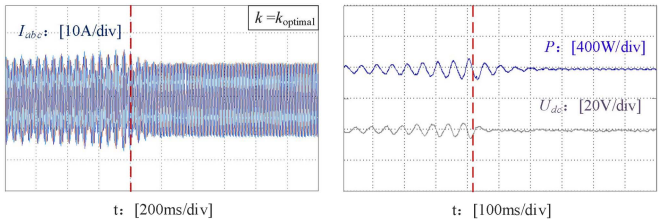

Fig. 19. Effect of equivalent hybrid synchronization control with a reasonable parameter ($k = k_{\mathrm{optimal}}$).

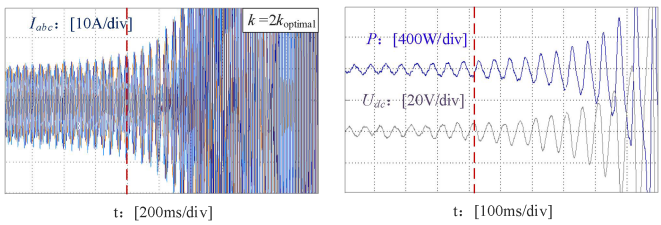

Fig. 20. Effect of equivalent hybrid synchronization control with an unreasonable parameter ($k = 2k_{\mathrm{optimal}}$).

When the line impedance is 16 mH and the output active power is 1.0 kW (SCR = 1.8), after increasing the PLL bandwidth from 20 Hz to 85 Hz, the GFL control converter shows significant distortion in the three-phase current and SSO with the frequency of 18 Hz in the active power.

With the introduction of equivalent hybrid power synchronization control during system oscillation, the three-phase current stabilizes rapidly, and the power oscillation is significantly suppressed. Moreover, the current exhibits a standard sine wave. Therefore, it is evident that the equivalent hybrid power synchronization method effectively suppresses the SSO induced by increasing the PLL bandwidth in the weak grid condition.

Figs. 18–20 show the experimental results of the three-phase current and active power with different values of k when the operation condition is the same as that in Fig. 17 (SCR = 1.8).

In Fig. 18, when $k = 0.5k_{\mathrm{optimal}}$, the oscillation amplitude of the three-phase current and active power is reduced, but the system still exhibits oscillations. In Fig. 19, when $k = k_{\mathrm{optimal}}$, the oscillations in three-phase current and active power are rapidly suppressed. In Fig. 20, when $k = 2k_{\mathrm{optimal}}$, the three-phase current and active power become unstable, which demonstrates that when the deviation of k from k_{optimal} is too large, the stability enhancement effect of the equivalent hybrid

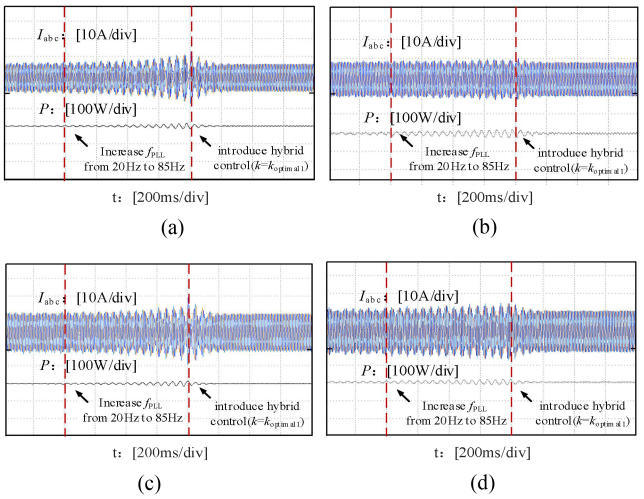

Fig. 21. Experimental results of GFL converters with a PLL bandwidth step change and then applying the equivalent hybrid control (with different active power). (a) $P = 0.9$ kW. (b) $P = 1.0$ kW. (c) $P = 1.2$ kW. (d) $P = 1.3$ kW.

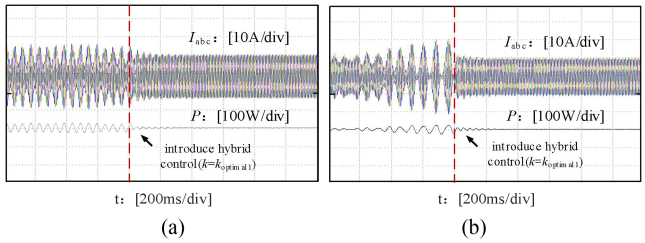

Fig. 22. Experimental results of GFL converters with a PLL bandwidth step change and then applying the equivalent hybrid control (with different L_g). (a) $L_g = 12$ mH. (b) $L_g = 18$ mH.

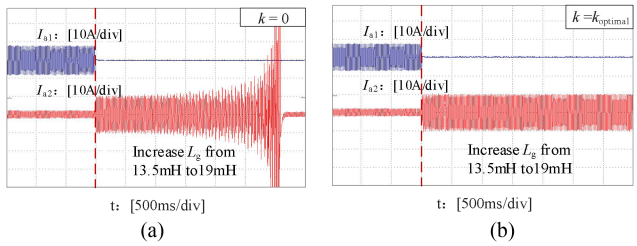

Fig. 23. Experimental results of a-phase current with and without the introduction of equivalent hybrid control when decreasing SCR suddenly. (a) $k = 0$. (b) $k = k_{\text{optimal}}$.

power synchronization control will be affected. Therefore, the parameters need to be reasonably selected within a certain range based on the selection criteria.

The parameter selection criteria proposed in this article provide certain guiding significance for improved control parameter design.

However, even when the selected parameters deviate somewhat from theoretical values, the equivalent hybrid dc IsynC still exhibits a notable stability enhancement effect. The transfer function in the improved control is a lead/lag function, which inherently possesses certain filtering and inertial characteristics. Therefore, the improved control parameters are not overly sensitive to conditional requirements. For instance, when the SCR changes, the improved control parameters selected under the original conditions can still achieve satisfactory performance.

To verify the feasibility of the equivalent hybrid control under different operating conditions, oscillation suppression experiments under various scenarios have been conducted for equivalent hybrid dc inertia control. In the experiment, the same improved control parameters were selected under different operating conditions to verify the effectiveness of the equivalent hybrid dc IsynC method. The experimental results are presented below. In Fig. 21, k_{optimal1} represents the theoretical value of the improved control parameters corresponding to the operating condition in Fig. 19.

Fig. 21(a)–(d) shows the grid-connected current and active power waveforms of the system under active power conditions of $P = 0.9$ kW, 1.0 kW, 1.2 kW, and 1.3 kW, after increasing the PLL bandwidth of the GFL control from 20 Hz to 85 Hz and then applying equivalent hybrid dc inertia control.

As shown in Fig. 21, when the PLL bandwidth is increased, the grid-connected current of the GFL inverter exhibits significant distortion, and the active power waveform generates SSOs at around 20 Hz. Upon introducing the equivalent hybrid power synchronization control during system oscillations, the inverter's grid current quickly stabilizes, power oscillations are significantly suppressed, and the current waveform becomes a sinusoidal signal. Due to differences in converter active power, the oscillation suppression effects vary slightly across the four cases, but the equivalent hybrid dc IsynC control can effectively mitigate the SSOs caused by the increased PLL bandwidth in different scenarios.

Fig. 22 shows the oscillation suppression experimental results under different line impedances. As shown in Fig. 22, when the PLL bandwidth is increased, the grid-connected current of the GFL inverter exhibits significant distortion, and the active power waveform generates SSOs. Upon introducing the equivalent hybrid power synchronization control during system oscillations, the inverter's grid current quickly stabilizes, power oscillations are significantly suppressed, and the current waveform becomes a sinusoidal signal. Due to differences in the line impedance, the oscillation suppression effects vary slightly across the 2 cases, but the equivalent hybrid dc IsynC control can effectively mitigate the SSOs caused by the increased PLL bandwidth in different scenarios.

To demonstrate that equivalent hybrid dc power control can enhance the system adaptability to weak grids, a SCR switching device was added based on the original line impedance. A parallel circuit consisting of $L_1 = 7$ mH and $L_2 = 2$ mH inductance was connected in series with the original line impedance of 12mH, placing the circuit breaker on the 2 mH branch. When the circuit breaker is closed, $L_{g1} = 13.5$ mH, and when the circuit breaker is open, $L_{g2} = 19$ mH.

Fig. 23 shows the experimental results of grid-connected three-phase current and active power when SCR is decreased suddenly. Fig. 23(a) and (b) shows the a-phase current waveforms of L_1 and L_2 when the grid-connected system applies GFL control and equivalent hybrid dc power control during SCR switching.

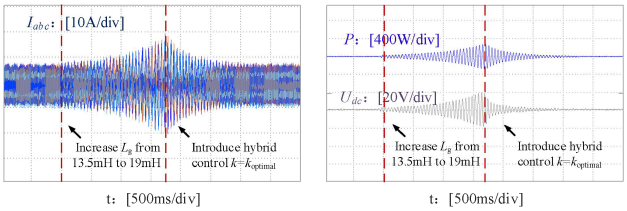

Fig. 24. Experimental results of grid current and active power when decreasing SCR and then introducing equivalent hybrid control.

As shown in Fig. 23(a), the grid-connected system using GFL control experiences a sudden increase in the a-phase current of L_1 after switching from $L_{g1} = 13.5$ mH (SCR $= 2.3$) to $L_{g2} =$ 19 mH (SCR $= 1.65$), leading to a divergent oscillation trend. The a-phase current of L_2 drops to zero instantaneously when the circuit breaker opens.

In contrast, Fig. 23(b) shows that the grid-connected system with equivalent hybrid dc power control maintains stability when switching from SCR $= 2.3$ to SCR $= 1.65$, allowing the system to operate stably. The a-phase current of L_2 also drops to zero when the circuit breaker opens. The comparative experiments verify that the proposed control can enhance the adaptability of GFL converters to the weak grid condition.

Fig. 24 shows the grid current and active power waveforms of the grid-connected system with equivalent hybrid power synchronization control applied when switching SCR from 2.3 to 1.65.

From Fig. 24, it is evident that the traditional GFL control system exhibits 18 Hz SSO and significant distortion in the grid current after switching SCR. However, after 1.75 s of oscillation, the introduction of equivalent hybrid dc power control leads to a decreasing trend in the SSO, and SSO is completely suppressed after 1 s. The grid current returns to a sinusoidal waveform, attesting to the effectiveness of equivalent hybrid dc power control in mitigating SSO triggered by SCR variations.

In summary, it is obvious that the proposed method can mitigate the SSO effectively in the weak grid. Moreover, the standards presented in Section IV can guide the selection for parameters of the equivalent hybrid synchronization method to some extent. Furthermore, the verification in more extreme conditions, such as a weaker grid, would be conducted in the future, and the application of the equivalent hybrid strategy with dc power synchronization on other occasions should be explored.

Currently, the principles and structures of existing improved control methods exhibit diversity, which leads to differences in implementation approaches, parameter design methods, and performance characteristics between existing methods and the proposed approach. Each method has its distinct features, and all contribute to enhancing the operational stability of grid-connected converters in weak grids.

VI. Conclusion

In this article, an equivalent hybrid control that combines GFL control with dc IsynC is proposed. After adding the proposed compensation term to the d-axis, the q-axis voltage, which is the input of the PLL will be consequently affected. As a result, the output of PLL will include the same component with dc IsynC, realizing the combination of GFL control and IsynC, and finally, the stability of the grid-connected system will be enhanced. Additionally, the parameter selection method of equivalent hybrid control has been concluded, making it convenient to implement in an application. Within the appropriate parameter range, the equivalent hybrid control strategy can enable the GFL control system to maintain stable operation in weak grid conditions. The effectiveness of the proposed method is verified by simulations and experiments.

The equivalent hybrid power control method presented in this article demonstrates good engineering adaptability. For the widely deployed GFL converters in current power systems, the method proposed in this study offers an improved solution that enhances control system stability in weak grids without altering the main circuit topology or the core control architecture. This method can be applied to grid-connected converter control systems incorporating a dc voltage loop, providing a new pathway to suppress SSOs in weak grids. In further research, it is necessary to conduct a comprehensive analysis aiming at the efficacy of the equivalent hybrid synchronization control in more extreme grid conditions and its application in the multiple-converter system.

References

[1] L. Zhang, L. Harnefors, and H.-P. Nee, "Power-synchronization control of grid-connected voltage-source converters," *IEEE Trans. Power Syst.*, vol. 25, no. 2, pp. 809–820, May 2010.

[2] J. Ma, L. Wang, and Y. Shen, "Interaction energy-based stability analysis method and application in grid-tied Type-4 wind turbine generator," *IEEE J. Emerg. Sel. Topics Power Electron.*, vol. 9, no. 5, pp. 5542–5557, Oct. 2021.

[3] X. Wang, M. G. Taul, Y. L. H. Wu, F. Blaabjerg, and L. Harnefors, "Grid-synchronization stability of converter-based resources—An overview," *IEEE Open J. Ind. Appl*, vol. 1, pp. 115–134, 2020, doi: 10.1109/OJIA.2020.3020392.

[4] L. Harnefors, X. Wang, A. G. Yepes, and F. Blaabjerg, "Passivity-based stability assessment of grid-connected VSCs—An overview," *IEEE J. Emerg. Sel. Topics Power Electron.*, vol. 4, no. 1, pp. 116–125, Mar. 2016.

[5] H. Liu, X. Xie, and W. Liu, "An oscillatory stability criterion based on the unified dq-frame impedance network model for power systems with high-penetration renewables," *IEEE Trans. Power Syst.*, vol. 33, no. 3, pp. 3472–3485, May 2018.

[6] J. F. Morris, K. H. Ahmed, and A. Egea-Alvarez, "Analysis of controller bandwidth interactions for vector-controlled VSC connected to very weak ac grids," *IEEE J. Emerg. Sel. Topics Power Electron.*, vol. 9, no. 6, pp. 7343–7354, Dec. 2021.

[7] M. G. Taul, C. Wu, S.-F. Chou, and F. Blaabjerg, "Optimal controller design for transient stability enhancement of grid-following converters under weak-grid conditions," *IEEE Trans. Power Electron.*, vol. 36, no. 9, pp. 10251–10264, Sep. 2021,.

[8] M. F. M. Arani and Y. A.-R. I. Mohamed, "Analysis and performance enhancement of vector-controlled VSC in HVDC links connected to very weak grids," *IEEE Trans. Power Syst.*, vol. 32, no. 1, pp. 684–693, Jan. 2017.

[9] D. Zhu, S. Zhou, X. Zou, and Y. Kang, "Improved design of PLL controller for LCL-type grid-connected converter in weak grid," *IEEE Trans. Power Electron.*, vol. 35, no. 5, pp. 4715–4727, May 2020.

[10] X. Li and H. Lin, "A design method of phase-locked loop for grid-connected converters considering the influence of current loops in weak grid," *IEEE J. Emerg. Sel. Topics Power Electron.*, vol. 8, no. 3, pp. 2420–2429, Sep. 2020.

[11] H. Gong, X. Wang, and L. Harnefors, "Rethinking current controller design for PLL-synchronized VSCs in weak grids," *IEEE Trans. Power Electron.*, vol. 37, no. 2, pp. 1369–1381, Feb. 2022.

[12] Z. Yang, C. Shah, T. Chen, J. Teichrib, and R. W. De Doncker, "Virtual damping control design of three-phase grid-tied PV inverters for passivity enhancement," *IEEE Trans. Power Electron.*, vol. 36, no. 6, pp. 6251–6264, Jun. 2021.
[13] A. Adib and B. Mirafzal, "Virtual inductance for stable operation of grid-interactive voltage source inverters," *IEEE Trans. Ind. Electron.*, vol. 66, no. 8, pp. 6002–6011, Aug. 2019.
[14] B. Hu, H. Nian, M. Li, Y. Xu, Y. Liao, and J. Yang, "Impedance-based analysis and stability improvement of DFIG system within PLL bandwidth," *IEEE Trans. Ind. Electron.*, vol. 69, no. 6, pp. 5803–5814, Jun. 2022.
[15] Z. Xie, Y. Chen, W. Wu, W. Gong, and J. M. Guerrero, "Stability enhancing voltage feed-forward inverter control method to reduce the effects of phase-locked loop and grid impedance," *IEEE J. Emerg. Sel. Topics Power Electron.*, vol. 9, no. 3, pp. 3000–3009, Jun. 2021.
[16] X. Zhang, M. Li, and D. Xu, "PCC voltage perturbation path analysis and compensation for grid-connected voltage-source converter under weak grid," *IEEE Trans. Ind. Electron.*, vol. 68, no. 12, pp. 12331–12339, Dec. 2021.
[17] K. M. Alawasa, Y. A.-R. I. Mohamed, and W. Xu, "Active mitigation of subsynchronous interactions between PWM voltage-source converters and power networks," *IEEE Trans. Power Electron.*, vol. 29, no. 1, pp. 121–134, Jan. 2014.
[18] C. Li, S. Wang, F. Colas, and J. Liang, "Dominant instability mechanism of VSI connecting to a very weak grid," *IEEE Trans. Power Syst.*, vol. 37,no. 1, pp. 828–831, Jan. 2022.
[19] F. Chen, L. Zhao, L. Harnefors, X. Wang, J. Kukkola, and M. Routimo, "Enhanced Q-axis voltage-integral damping control for fast PLL-synchronized inverters in weak grids," *IEEE Trans. Power Electron.*, vol. 39, no. 1, pp. 424–435, Jan. 2024.
[20] X. Lin, J. Yu, R. Yu, J. Zhang, Z. Yan, and H. Wen, "Improving small-signal stability of grid-connected inverter under weak grid by decoupling phase-lock loop and grid impedance," *IEEE Trans. Ind. Electron.*, vol. 69, no. 7, pp. 7040–7053, Jul. 2022.
[21] X. Lin, R. Yu, J. Yu, and H. Wen, "Constant-coupling-effect-based PLL for synchronization stability enhancement of grid-connected converter under weak grids," *IEEE Trans. Ind. Electron.*, vol. 70, no. 11, pp. 11310–11323, Nov. 2023.
[22] M. Z. Mansour, M. H. Ravanji, A. Karimi, and B. Bahrani, "Small-signal synchronization stability enhancement of grid-following inverters via a feedback linearization controller," *IEEE Trans. Power Del.*, vol. 37, no. 5, pp. 4335–4344, Oct. 2022.
[23] L. Huang et al., "A virtual synchronous control for voltage-source converters utilizing dynamics of DC-link capacitor to realize self-synchronization," *IEEE J. Emerg. Sel. Topics Power Electron.*, vol. 5, no. 4, pp. 1565–1577, Dec. 2017.
[24] S. Sang, C. Zhang, X. Cai, M. Molinas, J. Zhang, and F. Rao, "Control of a Type-IV wind turbine with the capability of robust grid-synchronization and inertial response for weak grid stable operation," *IEEE Access*, vol. 7, pp. 58553–58569, 2019.
[25] Y. Qin, H. Wang, Z. Deng, J. Zhang, R. Yang, and X. Cai, "Control of inertia-synchronization controlled wind turbine generators under symmetrical grid faults," *IEEE Trans. Energy Convers.*, vol. 38, no. 2, pp. 1085–1096, Jun. 2023.
[26] L. Harnefors, J. Kukkola, M. Routimo, M. Hinkkanen, and X. Wang, "A universal controller for grid-connected voltage-source converters," *IEEE J. Emerg. Sel. Topics Power Electron.*, vol. 9, no. 5, pp. 5761–5770, Oct. 2021.
[27] P. Liu, X. Xie, and J. Shair, "Adaptive hybrid grid-forming and grid-following control of IBRs with enhanced small-signal stability under varying SCRs," *IEEE Trans. Power Electron.*, vol. 39, no. 6, pp. 6603–6607, Oct. 2024.
[28] T. Liu and X. Wang, "Physical insight into hybrid-synchronization-controlled grid-forming inverters under large disturbances," *IEEE Trans. Power Electron.*, vol. 37, no. 10, pp. 11475–11480, Oct. 2022.
[29] L. A. M. Lima and E. H. Watanabe, "Hybrid control scheme for VSC presenting both grid-forming and grid-following capabilities," *IEEE Trans. Power Del.*, vol. 37, no. 6, pp. 4570–4581, Dec. 2022.
[30] F. Han, X. Zhang, M. Li, F. Li, and W. Zhao, "Stability control for grid-connected inverters based on hybrid-mode of grid-following and grid-forming," *IEEE Trans. Ind. Electron.*, vol. 71, no. 9, pp. 10750–10760, Sep. 2024.

Ruixun Ma was born in Heilongjiang Province, China, in 2000. She received the B.S. and M.S. degrees in electrical engineering from the Harbin Institute of Technology, Harbin, China, in 2022 and 2025, respectively.

Her research interests include the modeling and stability analysis of renewable energy conversion systems.

Xueguang Zhang (Member, IEEE) was born in Heilongjiang Province, China, in 1981. He received the B.S., M.S., and Ph.D. degrees in electrical engineering from the Harbin Institute of Technology, Harbin, China, in 2003, 2005, and 2010, respectively.

Since 2020, he has been a Professor with the Department of Electrical and Engineering, Harbin Institute of Technology. His research interests include distributed power generation and renewable energy conversion systems.

Dianguo Xu (Fellow, IEEE) was born in Heilongjiang Province, China, in 1960. He received the B.S. degree in control engineering from Harbin Shipbuilding Engineering Institute, Harbin, China, in 1981, and the M.S. and Ph.D. degrees in electrical engineering from the Harbin Institute of Technology, Harbin, China, in 1984 and 1990, respectively.

Since 1994, he has been a Professor with the Department of Electrical Engineering, Harbin Institute of Technology. His research interests include robotics, lighting electronics, power quality mitigation, consumer electronics, power electronics, and motor drives.